Journal of
Composites Science

MDPI

Article

Design of Experiments (DoE) Approach for Optimizing the Processing and Manufacturing Parameters of SnO_2 Thin Films via Ultrasonic Pyrolytic Deposition

Aldo Enrique Mariño-Gámez [1], Maria Eugenia Juarez-Huitron [1], Josúe Amilcar Aguilar-Martínez [1,*], Luis Felipe-Verdeja [2], Linda Viviana García-Quiñonez [3] and Cristian Gómez-Rodríguez [4,*]

[1] Centro de Investigación e Innovación en Ingeniería Aeronáutica (CIIIA), Facultad de Ingeniería Mecánica y Eléctrica, Universidad Autónoma de Nuevo León, Carretera a Salinas Victoria km. 2.3, Apodaca 66600, Nuevo Leon, Mexico; aldo.marinogmz@uanl.edu.mx (A.E.M.-G.); mjuarezho@uanl.edu.mx (M.E.J.-H.)
[2] Departamento de Ciencia de los Materiales e Ingeniería Metalúrgica, Escuela de Minas, Energía y Materiales, Universidad de Oviedo, 33004 Oviedo, Asturias, Spain; lfv@uniovi.es
[3] Centro de Investigación en Recursos Energéticos y Sustentables (CIRES), Universidad Veracruzana, Av. Universidad Veracruzana km 7.5, Col. Santa Isabel I, Coatzacoalcos 96538, Veracruz, Mexico; lingarcia@uv.mx
[4] Departamento de Mecánica, Facultad de Ingeniería, Campus Coatzacoalcos, Universidad Veracruzana, Av. Universidad km 7.5, Col. Santa Isabel, Coatzacoalcos 6535, Veracruz, Mexico
* Correspondence: josue.aguilarmrt@uanl.edu.mx (J.A.A.-M.); crisgomez@uv.mx (C.G.-R.)

Abstract

This work employed a design-of-experiments (DoE) strategy, specifically a 2^3 full factorial design, to assess how suspension concentration (0.001–0.002 g/mL), substrate temperature (60–80 °C), and deposition height (10–15 cm) influence tin dioxide (SnO_2) thin films produced by ultrasonic spray pyrolysis (USP). The response variable was the net intensity of the principal diffraction peak, used as an operational metric for detecting the deposited phase. All patterns matched the SnO_2 phase cassiterite reference without impurity peaks. Statistical analyses (ANOVA, Pareto and half-normal plots, and response surface methodology, RSM) identified suspension concentration as the most influential factor, followed by significant two- and three-factor interactions. The model exhibited a high coefficient of determination (R^2 = 0.9908) and low standard deviation (12.53), validating its predictive capability. The optimal deposition process was achieved at the highest suspension concentration (0.002 g/mL), lowest substrate temperature (60 °C), and shortest deposition height (10 cm). These results demonstrate the utility of full factorial DoE for quantifying and controlling deposition outcomes in USP and provide a robust statistical framework to guide the synthesis of SnO_2 thin films.

Keywords: modeling; processing and manufacturing; ultrasonic spray pyrolysis; x-ray diffraction; tin dioxide; thin films

Academic Editor: Francesco Tornabene

Received: 7 August 2025
Revised: 21 September 2025
Accepted: 1 October 2025
Published: 10 October 2025

Citation: Mariño-Gámez, A.E.; Juarez-Huitron, M.E.; Aguilar-Martínez, J.A.; Felipe-Verdeja, L.; García-Quiñonez, L.V.; Gómez-Rodríguez, C. Design of Experiments (DoE) Approach for Optimizing the Processing and Manufacturing Parameters of SnO_2 Thin Films via Ultrasonic Pyrolytic Deposition. *J. Compos. Sci.* **2025**, *9*, 555. https://doi.org/10.3390/jcs9100555

1. Introduction

The deposition of semiconducting materials in thin film form has attracted considerable attention over the years due to its demand in areas such as microelectronics [1], display technologies [2], energy conversion [3], and storage systems [4]. Among these materials, tin(IV) oxide (SnO_2) thin films have been particularly attractive due to their electron transport capacity [5], and their environmental stability [6]. The SnO_2 is an *n*-type semiconductor with tetragonal crystalline geometry, characterized by a wide band gap of approximately 3.6 eV, high intrinsic donor density, and thermal stability [7–10]. These

properties make SnO_2-based composite films highly suitable for a range of technological applications, including solar cells [11], memory devices [12], gas sensors [13], optoelectronics [14], and spintronic applications [15]. In many of these applications, the performance of SnO_2 thin films is closely linked to their crystallographic structure, which in turn is strongly influenced by the deposition parameters [16,17]. Therefore, controlling and optimizing deposition parameters is essential to tailor film properties to meet specific functional requirements [18,19]. Traditionally, the one variable at a time (OVAT) method has been used to investigate the influence of individual deposition parameters [20]. Although straightforward, this approach is inefficient, time-consuming, and incapable of detecting interaction effects between variables, which are often critical in complex deposition processes [21]. To overcome these limitations, design of experiments (DoE) methodologies have been increasingly adopted as statistically rigorous approaches for evaluating and optimizing multiple variables simultaneously [22]. DoE approaches enable efficient experimental planning, minimize the number of required experiments, and provide insights into both main effects and interaction effects among process parameters [23]. This makes them particularly suitable for guiding material synthesis in systems where multiple interdependent variables influence the outcome [24]. Several researchers have successfully applied DoE methodologies to SnO_2 thin film deposition processes. For instance, Pinheiro [25] utilized a fractional factorial design to identify optimal spray volume and fluorine-to-tin precursor ratio in the fabrication of fluorine-doped tin oxide films via spray pyrolysis for photovoltaic applications. Patel, Vaghela, and Gohel [26] employed a Box-Behnken design oriented multi-response optimization of spray-coated SnO_2 thin films, utilizing response surface methodology (RSM) to model and predict deposition results. In another study, Cruz et al. [27] applied a Taguchi design to investigate the effect of deposition parameters on the physical and chemical properties of SnO_2 films used in dye-sensitized solar cells. Similarly, Chianeh and Basiri [28] adopted a Box–Wilson also called central composite design (CCD) to model and evaluate the influence of process variables on the efficiency of azo dye removal using nano-SnO_2 film depositions while Tilebon and Norouzbeigi [29] used ANOVA-based statistical analysis to identify significant factors affecting the wettability of surfaces deposited with SnO_2. Despite these studies demonstrate the effectiveness of design of experiments (DoE) in optimizing various SnO_2 deposition techniques, limited research has been conducted on its application to ultrasonic spray pyrolysis (USP), a method that stands out for its operational simplicity, low cost, and compatibility with environmentally benign precursors compared to conventional techniques such as atmospheric pressure solvothermal (APS) [30], electron beam physical vapour deposition (EBPVD) [31], and chemical bath deposition (CBD) [32] To address this research gap, the present study investigates the effects of three key deposition parameters, suspension concentration, substrate temperature, and deposition height, on the structural characteristics of SnO_2 thin films fabricated via ultrasonic spray pyrolytic deposition. A 2^3 full factorial DoE was employed to analyze the individual and interaction effects of these variables on the developed film. The results revealed that the concentration of the suspension was the most influential parameter, exhibiting a strong positive correlation with with the response variable, as quantified by the net peak intensity in the X-ray diffraction (XRD) profiles. Substrate temperature and deposition height showed weaker but statistically significant effects, and their interaction produced a synergistic contribution. A significant three-factor interaction was also identified, indicating the nonlinear nature of the process. The developed statistical model achieved a high coefficient of determination (R^2 = 0.9908), confirming its predictive accuracy. These findings suggest that optimizing the USP process requires not only adjusting individual parameters, particularly the concentration of the suspension, but also managing their interactions. The results contribute to a more comprehensive understanding

of the deposition process and offer a quantitative framework for synthesizing SnO_2 films with controlled crystallographic properties suitable for advanced functional applications.

2. Materials and Methods

2.1. Deposition Process

In this study, SnO_2 powder was used as the starting material for the suspension at concentrations of 0.001 and 0.002 g/mL and distilled water was employed as the auxiliary liquid agent. All reagents were purchased from Sigma-Aldrich (Burlington, MA, USA). The suspension was homogenized at room temperature using a planetary micro ball mill (Fritsch Pulverisette 7 Classic Line, Pittsboro, NC, USA), with a 12 mL agate (SiO_2) container and six agate balls (10 mm diameter, 1.39 g each, total mass of 8.34 g). The milling parameters were set to a rotational speed of 300 rpm, with each cycle lasting 5 min, followed by a direction reversal. A total of 11 cycles were conducted, resulting in 60 min of effective milling time. For the two levels of suspension concentration (0.001 and 0.002 g/mL) and a working volume of 12 mL, the solid masses were 0.012 g and 0.024 g, respectively, corresponding to ball-to-powder ratios (BPR) of ≈695:1 and ≈348:1. Agate was used as it is a chemically inert material, minimizing contamination. The deposition process was carried out at a spray rate of 50 mL/h, with a working power of 2 W and a frequency of 108 kHz. These parameters were kept constant, as they are part of the technical specifications of the ultrasonic generator used in the deposition system. The substrate used was SiO_2 with dimensions of 25 × 75 × 1.3 mm. The substrate temperature was varied between 60 °C and 80 °C, the nozzle-to-substrate distance was set to either 10 cm or 15 cm, and the SnO_2 concentration was maintained at either 0.001 or 0.002 g/mL, according to the experimental design. The response variable was defined as the intensity (a.u.) of the main diffraction peak in the X-ray diffraction (XRD) profiles of the deposited films. XRD analyses were performed using a PANalytical Empyrean diffractometer (Malvern, UK) in grazing incidence mode, employing CoKα radiation ($\lambda = 1.78901$ Å) at an operating voltage of 40 kV and a current of 40 mA. Data were collected over a 2θ range of 20–100°, with an omega angle of 0.2°, a step size of 0.02°, and a counting time of 10 s per step in continuous scan mode.

2.2. Experimental Design

The optimization of the process parameters for obtaining the films was carried out using a statistical approach based on a full factorial 2^k design. In this study, a 2^3 factorial design with two replicates was employed (resulting in a total of 16 samples), considering three critical factors: suspension concentration (g/mL) (X_1) , substrate temperature (°C) (X_2), and deposition height (cm) (X_3). A summary of the experimental factors involved in the ultrasonic spray pyrolysis (USP) process, along with their assigned low and high levels, is provided in Table 1. For each combination of process settings, the intensity of the main peak in the X-ray diffraction (XRD) patterns of the 16 films was recorded as the response variable.

Table 1. Factors and levels of the 2^3 full factorial design.

Variable	USP Process Factors	Units	Low Level (−1)	High Level (+1)
X_1	Concentration	g/mL	0.001	0.002
X_2	Temperature	°C	60	80
X_3	Height	cm	10	15

In this study, the 2^3 full factorial design demonstrated a high statistical power of 95.6%, calculated using two replicates and a signal-to-noise ratio (S/N) of 2.

3. Results

3.1. Response Variable (X-Ray Diffraction)

The diffraction profiles obtained by grazing incidence for the 16 films synthesized under varying process conditions are shown in Figure 1.

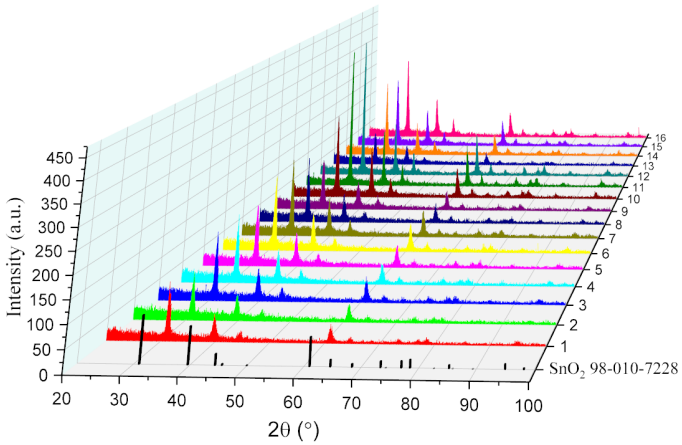

Figure 1. Diffraction profiles of the 16 films obtained via ultrasonic spray pyrolysis.

The reference diffraction pattern from ICDD PDF # 98-010-7228 for SnO_2 was used to confirm the phase composition of the samples. No secondary phases or impurity peaks were detected in any of the films, indicating successful deposition of pure SnO_2 across all experimental conditions. For each profile, the principal diffraction peak corresponding to SnO_2 was identified, and its net peak height expressed in arbitrary units (a.u.) was determined. The net peak height of the intensity, determined from the baseline to the maximum using a parabolic fitting method, was selected as the response variable for the experimental design.

3.2. Design Disposition

Table 2 summarizes the design disposition, including the encoded levels of the process factors and the response variable, Intensity (a.u.) (Y), recorded for each process setting combination with its replicate (totaling 16 films).

Table 2. Full factorial 2^3 design disposition for the parameters.

Run	X_1	X_2	X_3	Y
				Intensity (a.u.)
1	−1	1	−1	103.9
2	−1	1	1	80.2
3	−1	−1	−1	135.4
4	−1	−1	1	127.8
5	−1	−1	−1	130.8
6	1	−1	1	175.4
7	1	−1	1	177.4
8	−1	1	−1	148.5

Table 2. *Cont.*

Run	X_1	X_2	X_3	Y
				Intensity (a.u.)
9	−1	−1	1	117.9
10	1	1	1	213.6
11	1	−1	−1	396.6
12	1	−1	−1	400.2
13	−1	1	1	81.6
14	1	1	−1	206.9
15	1	1	−1	195.5
16	1	1	1	229.6

3.3. DoE Analysis

The Figure 2 shows a correlation grid for the preliminary analysis of the design of experiments (DoE), which considers the three factors and the response variable. The grid is color-shaded to visually represent the degree of correlation between each variable, where red indicates a strong positive correlation and blue indicates a negative correlation. The numerical values in each cell provide an accurate quantification of the correlation coefficients.

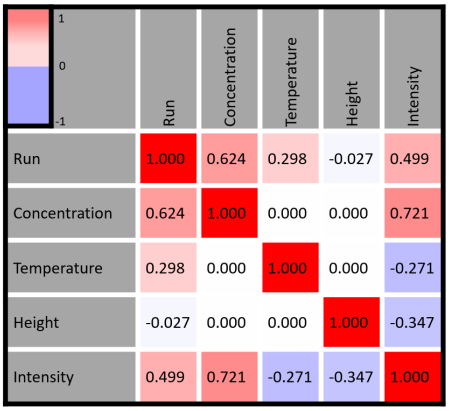

Figure 2. Correlation grid among the three process factors and the response variable.

Among the evaluated factors, the concentration of the suspension (X_1) exhibits the strongest correlation with the response variable, with a coefficient of 0.721, indicating a notable direct association between the two. In contrast, substrate temperature (X_2) and deposition height (X_3) present lower correlation coefficients of −0.271 and −0.347, respectively. The factors exhibited distinct trends, concentration had a positive effect, while substrate temperature and deposition height displayed negative effects. An increase in the concentration of the suspension is likely to raise the amount of cassiterite (SnO_2) delivered to the substrate, promoting denser packing or preferred orientation, which in turn increases the measured XRD peak intensity. By contrast, higher substrate temperatures can accelerate solvent evaporation before or at impact, yielding less uniform coverage and a reduction in the observed intensity. Subsequently, scatter plots were plotted to investigate the relationship between the response variable (Intensity) and the concentration of the suspension, while also accounting for stratification according to two critical process factors, specifically the deposition height and the substrate temperature, as illustrated in Figure 3.

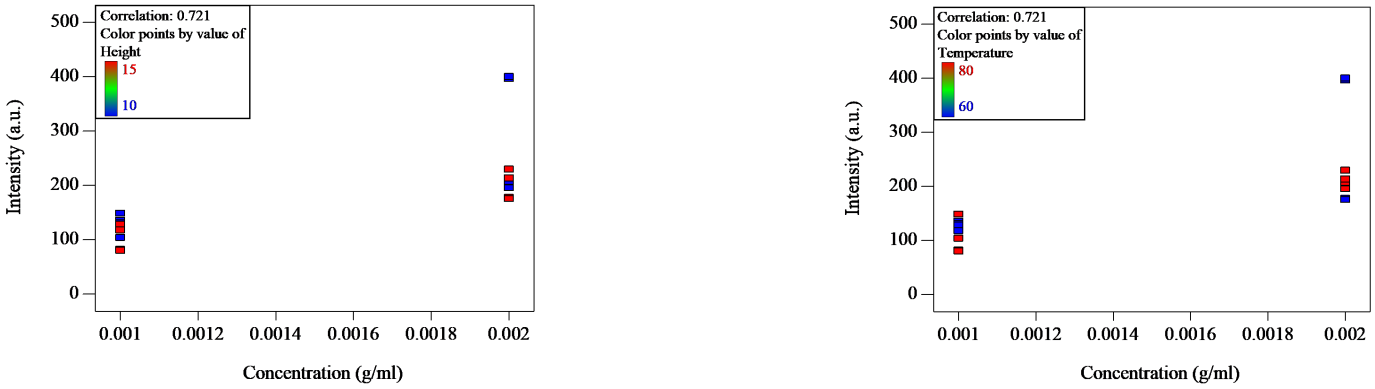

Figure 3. Scatter plots showing the relationship between intensity and suspension concentration, with color indicating (**a**) deposition height and (**b**) substrate temperature.

Each point on the plots corresponds to the measured intensity associated with a specific combination of experimental conditions, with color differentiation used to indicate the respective levels of height (Figure 3a) and substrate temperature (Figure 3b). In Figure 3a, where color represents deposition height, a clear stratification is observed at both low (0.001 g/mL) and high (0.002 g/mL) concentrations. Films deposited at the shorter nozzle–substrate distance (10 cm) exhibit higher intensities than those at 15 cm, consistent with greater delivered mass/coverage of cassiterite (SnO_2) and/or stronger preferred orientation at reduced spray distances. This trend is attributable to more efficient delivery of solids to the substrate and reduced loss of deposit during transport, which favor continuous coverage and texture development. In contrast, Figure 3b) displays stratification based on substrate temperature. At lower concentrations of the suspension, films deposited at 60 °C exhibit slightly higher intensity values compared to those synthesized at 80 °C. At higher concentrations, although the difference becomes less pronounced, a general trend of decreasing intensity with increasing substrate temperature remains evident. This behavior likely reflects changes in evaporation kinetics and surface redistribution at higher temperatures that lessen local continuity and attenuate the diffracted signal. Nevertheless, these scatter plot observations represent a preliminary assessment; a more comprehensive analysis of the factor interactions will be discussed subsequently. Figure 4 presents the half-normal probability plot for the standardized effects of the process factors (X_1 = A, X_2 = B, X_3 = C) and their interactions on the response variable (Intensity).

This graphical tool assists in distinguishing significant effects from random experimental noise based on their deviation from the reference line. In the plot, green triangles represent pure error estimates, while the colored squares denote the main effects and factor interactions. Data points deviating markedly from the red reference line are considered to have substantial influence on the response. Among the evaluated factors, the concentration of the suspension (A) exhibited the strongest effect, located furthest from the reference line, highlighting its dominant positive impact on intensity value. This finding is consistent with the preliminary correlation analysis, where concentration showed the highest correlation with net intensity of the principal diffraction peak. Regarding the interactions of two factors, AB, AC, and BC were observed, with the BC interaction (temperature and height) standing out, though its magnitude was smaller compared to factor A. The positive standardized effect of BC suggests that the simultaneous increase of temperature and height results in higher diffracting intensity. In contrast, AC and AB interactions exhibited negative standardized effects, implying that a concurrent increase in concentration with height or temperature leads to decreased intensity values. Although AC and AB lie closer to the

baseline, they remain distinguishable from pure error, indicating moderate but notable influences. The three-factor interaction ABC also appears among the significant terms, suggesting that the simultaneous variation of concentration, temperature, and height plays a role in determining the final intensity values. The presence of higher-order interactions highlights the complexity of the ultrasonic spray pyrolysis process, emphasizing that the behavior of the response cannot be fully understood without considering the interdependence between process variables. To visualize the magnitude of all the effects of the process and their interactions on the crystal structure of SnO_2 films, a Pareto chart was created, as shown in Figure 5.

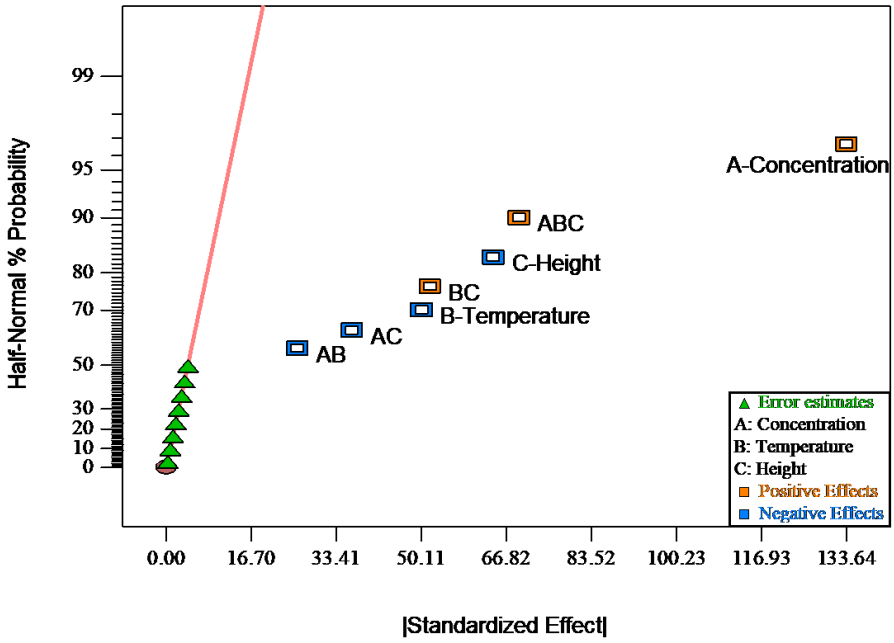

Figure 4. Half -normal probability plot of standardized effects.

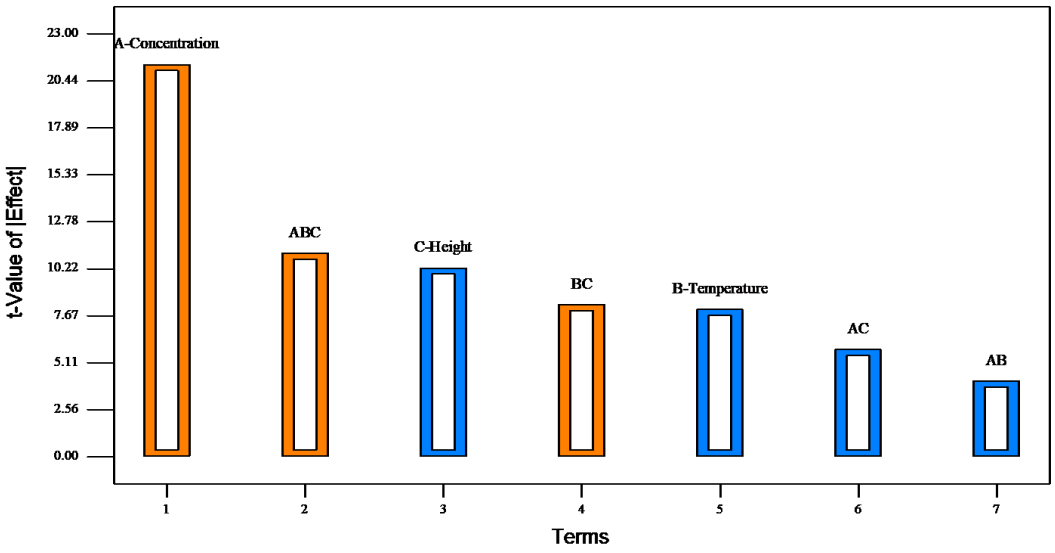

Figure 5. Pareto chart illustrating the magnitude of the effects.

The chart arranges the effects according to their absolute t values, a dimensionless metric that normalizes each effect relative to its associated standard deviation. This rep-

resentation allows for a direct comparison between the individual parameters and their interactions. As expected, concentration (A) appears as the most influential parameter, in agreement with the results obtained from the correlation analysis and the half-normal plot. The interaction involving all three factors ABC also shows a considerable magnitude, indicating that the combined variation of concentration, substrate temperature, and deposition height contributes significantly to the structural characteristics of SnO_2 films. While individual effects such as deposition height (C) and substrate temperature (B) are less pronounced, their interactions in particular BC demonstrate the complex nature of the deposition process, in which the response is influenced by the interaction of multiple variables, rather than by isolated parameter changes alone.

The statistical evaluation of the effects included in the predictive model was conducted through an analysis of variance (ANOVA), as presented in Table 3.

Table 3. Analysis of variance (ANOVA) for selected factorial model.

Term	Coefficient	SS	df	Mean Square	F-Value	*p*-Value *
Model		1.360×10^5	7	19434.06	123.72	<0.0001
b_0	182.58					
X_1	66.82	71,435.93	1	71,435.93	454.79	<0.0001
X_2	−25.11	10,085.18	1	10,085.18	64.21	<0.0001
X_3	−32.14	16,531.53	1	16,531.53	105.25	<0.0001
X_1X_2	−12.89	2659.98	1	2659.98	16.93	0.0034
X_1X_3	−18.26	5332.65	1	5332.65	33.95	0.0004
X_2X_3	25.92	10,748.51	1	10,748.51	68.43	<0.0001
$X_1X_2X_3$	34.68	19,244.63	1	19,244.63	122.52	<0.0001
Pure Error		1256.60	8	157.08		
Corrected Total		1.373×10^5	15			
Std. Dev.	12.53	R-Squared		0.9908		
Mean	182.58	Adj R-Squared		0.9828		
C.V.%	6.86	Pred R-Squared		0.9634		
PRESS	5026.42	Adeq Precision		35.826		

* *p*-Values less than 0.05 indicate model terms are significant.

The F-value associated with the model is 123.72, with a corresponding *p*-value of 0.0001, indicating that the model is statistically significant and that the likelihood of such a result arising from random variation is less than 0.01%. All investigated terms, including the individual factors (X_1, X_2, X_3), the two-factor interactions (X_1X_2, X_1X_3, X_2X_3), and the three-factor interaction ($X_1X_2X_3$), exhibit *p*-values below 0.05, confirming their statistical significance and relevance to the response variable. The model also shows strong predictive performance, as evidenced by an adjusted R-squared value of 0.9828 and a predicted R-squared of 0.9634. The small difference between these values (less than 0.2) reflects the robustness of the model and the absence of overfitting. Additionally, the model's adequate precision value of 35.826 far exceeds the commonly accepted minimum of 4, indicating a high signal-to-noise ratio and reinforcing the model's capacity to effectively navigate the design space. The final equations in terms of coded factors were:

$$Y = 182.58 + 66.82X_1 - 25.11X_2 - 32.14X_3 - 12.89X_1X_2 - 18.26X_1X_3 + 25.92X_2X_3 + 34.68X_1X_2X_3 \quad (1)$$

Also, the cube plot in Figure 6 displays the model's predicted response as a function of the three significant factors: X_1, X_2, and X_3.

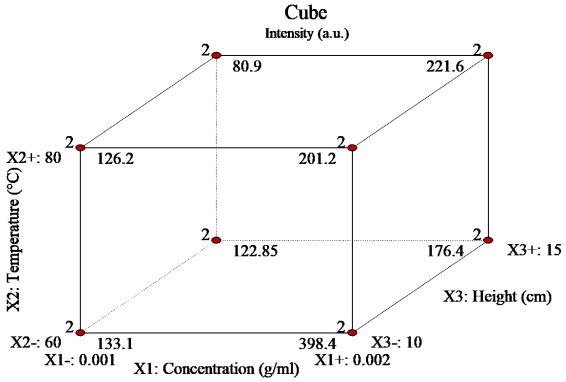

Figure 6. Cube plot of the coded model.

The highest predicted diffracted intensity (398.4 a.u.) occurs at the combination X_1+, X_2-, and X_3- (lower right front corner). This outcome is interpreted as a larger amount of cassiterite phase effectively deposited and/or a stronger preferred orientation on the substrate. On the other hand, response surface methodology (RSM) and contour plots in Figure 7 illustrate the influence of the suspension concentration, substrate temperature, and deposition height on the intensity of the diffracted peak, used as the response variable.

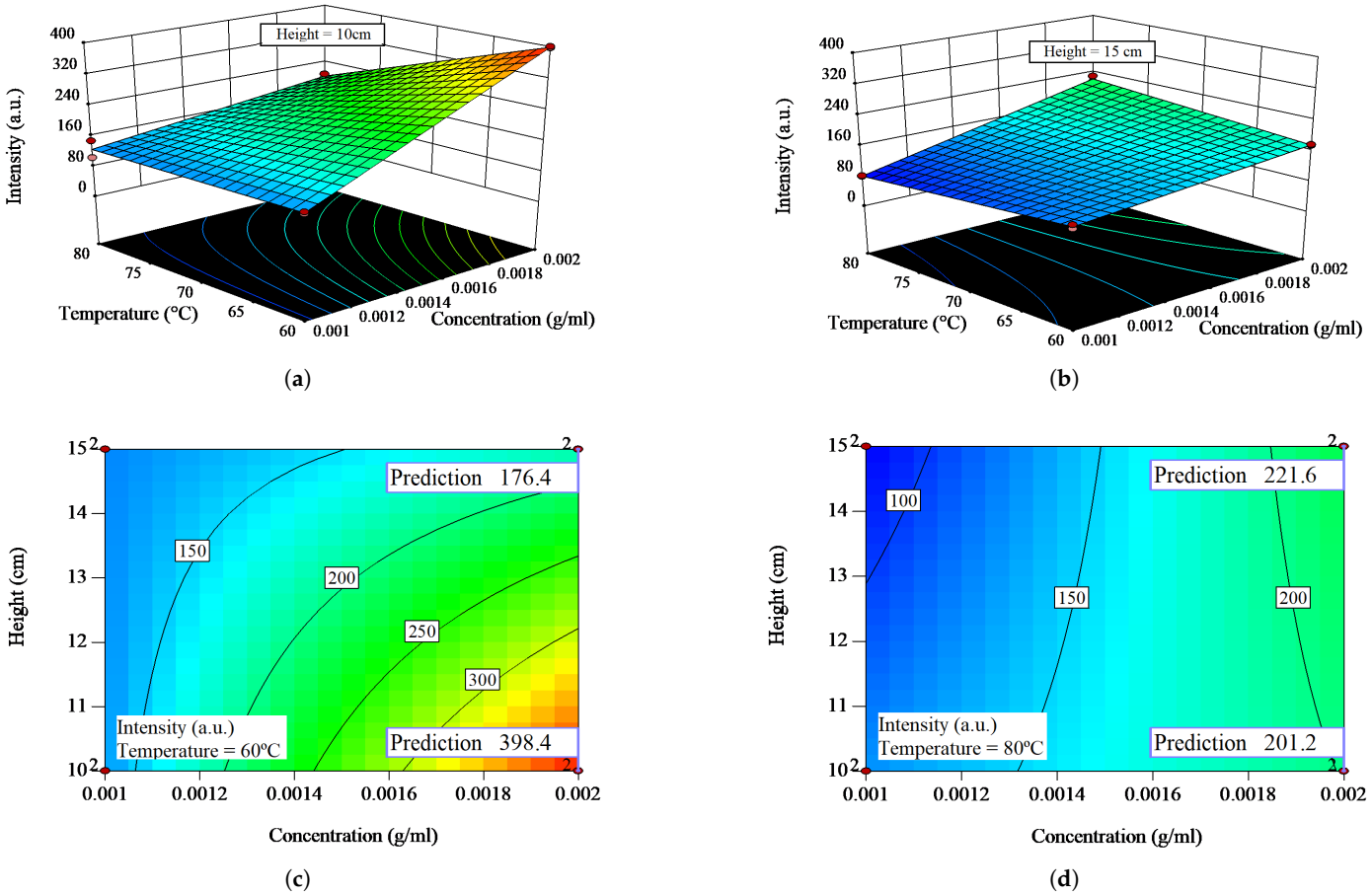

Figure 7. Response surface and contour plots for intensity as the response variable. (**a**) Response surface plot showing the interaction between the concentration of the suspension and the substrate temperature at a lower deposition height (10 cm). (**b**) Response surface plot showing same interaction at a higher deposition height (15 cm). (**c**) Contour plot illustrating the interaction between concentration and deposition height at lower temperature (60 °C). (**d**) Contour plot illustrating same interaction at higher temperature (80 °C).

In 3D Surface plots (a) and (b), where the interaction between suspension concentration and substrate temperature is evaluated at two fixed heights (10 cm and 15 cm), a consistent trend is observed: higher diffraction intensities are associated with increased suspension concentration, particularly at lower substrate temperatures and reduced deposition heights. This indicates that more concentrated microdroplets deliver a greater amount of SnO_2 (cassiterite) to the substrate. In the contour plots (c) and (d), which examine the interaction between concentration and deposition height at fixed substrate temperatures (60 °C and 80 °C), the response surface shows a stronger gradient at 60 °C, where intensity increases markedly with decreasing height and increasing concentration. At 80 °C, the response surface becomes flatter, reflecting reduced sensitivity of the deposited phase intensity under faster solvent evaporation conditions. These results confirm that concentration is the dominant factor, while substrate temperature and deposition height act as modulators of deposition efficiency and texture development in USP-grown SnO_2 films.

4. Conclusions

This study, based on a 2^3 full factorial design of experiments (DoE), enabled the rigorous evaluation and optimization of the effects of suspension concentration (X_1), substrate temperature (X_2), and deposition height (X_3) on the structural properties of SnO_2 thin films deposited via ultrasonic spray pyrolysis (USP). All conditions confirmed the preservation of a single-phase cassiterite structure without secondary phases or impurities. Statistical analyses consistently identified suspension concentration (X_1) as the dominant factor, showing a strong positive correlation with intensity (r = 0.721), an ANOVA F-value of 454.79, and a highly significant p-value (<0.0001). This effect is primarily associated with the greater solid load delivered by concentrated droplets, which enhances the effective coverage and texture of the deposited layer. In contrast, substrate temperature (X_2) and deposition height (X_3) exhibited weaker individual effects, with negative correlation coefficients (r = -0.271 and -0.347, respectively), yet both significantly modulated deposition efficiency through their interactions. In particular, the X_2X_3 interaction showed a strong positive influence (F = 68.43, $p < 0.0001$), indicating that higher temperatures can counterbalance evaporation losses at larger spray heights, improving effective deposition. The three-factor interaction ($X_1X_2X_3$) was also significant (F = 122.52, $p < 0.0001$), highlighting the nonlinear complexity of the process where the optimal effective amount of deposited material depends on the combined tuning of all three parameters. The Pareto and half-normal plots confirmed that suspension concentration (X_1) and the three-factor interaction ($X_1X_2X_3$) were the most influential contributors to the variation in deposited phase intensity. Model validation yielded a high coefficient of determination (R^2 = 0.9908) and a low standard deviation (12.53), confirming its predictive capability. Response surface methodology (RSM) indicated that the optimal condition for maximizing XRD intensity was achieved at the highest suspension concentration (0.002 g/mL), lowest substrate temperature (60 °C), and shortest deposition height (10 cm). These results demonstrate that the efficiency of SnO_2 deposition via USP and the resulting XRD response, are primarily governed by the concentration of the suspension and modulated by the coupled effects of substrate temperature and deposition height. This study establishes a quantitative framework for controlling and optimizing ultrasonic spray pyrolysis of SnO_2 films to meet diverse technological requirements and serves as a point of departure for extending the DoE approach to SnO_2-based composite architectures.

Author Contributions: Conceptualization, A.E.M.-G. and J.A.A.-M.; methodology, A.E.M.-G. and L.V.G.-Q.; software, A.E.M.-G. and C.G.-R.; validation, A.E.M.-G., M.E.J.-H. and J.A.A.-M.; formal analysis, A.E.M.-G. and L.V.G.-Q.; investigation, A.E.M.-G.; resources, A.E.M.-G.; data curation, C.G.-R. and L.V.G.-Q.; writing—original draft preparation, A.E.M.-G.; writing—review and editing, L.F.-V.; visualization, C.G.-R.; supervision, J.A.A.-M. and C.G.-R.; project administration, M.E.J.-H.; funding acquisition, L.V.G.-Q. All authors have read and agreed to the published version of the manuscript.

Funding: This research received no external funding.

Data Availability Statement: The data presented in this study are available within the article.

Acknowledgments: L.V. García-Quiñonez sincerely acknowledge CONAHCYT-SECIHTI (Proyecto Ciencia Basica y de Frontera—CBF2023-205-657).

Conflicts of Interest: The authors declare no conflicts of interest.

Abbreviations

The following abbreviations are used in this manuscript:

SnO_2	Tin(IV) oxide
DoE	Design of Experiments
OVAT	One Variable At a Time
RSM	Response Surface Methodology
CCD	Central Composite Design
USP	Ultrasonic Spray Pyrolysis
APS	Atmospheric Pressure Solvothermal
EBPVD	Electron Beam Physical Vapor Deposition
CBD	Chemical Bath Deposition
XRD	X-ray Diffraction
ANOVA	Analysis of Variance
SS	Sum of Squares
df	Degrees of Freedom
Std. Dev.	Standard Deviation
C.V.%	Coefficient of Variation (Percentage)
PRESS	Predicted Residual Sum of Squares
R-Squared (R^2)	Coefficient of Determination
Adj R-Squared	Adjusted R-Squared
Pred R-Squared	Predicted R-Squared
Adeq Precision	Adequate Precision
X_1	Suspension Concentration (g/mL)
X_2	Substrate Temperature (°C)
X_3	Deposition Height (cm)
Y	Response variable (Net peak intensity in XRD, a.u.)
b_0	Mean value of responses across all experiments

References

1. Wang, F.; Lv, Z.; Zhong, X.; Wang, J.; Li, F.; Chen, H.; Li, M. Soft-template-assisted bottom-up fabrication of tunable porosity monolithic copper film for interconnection in microelectronics. *J. Taiwan Inst. Chem. Eng.* **2023**, *152*, 105192. [CrossRef]
2. Ahn, K.; Islam, M.M.; Chang, Y.; Jang, J. Highly Robust Spray-Pyrolyzed Al_2O_3 Gate Insulator for Flexible a-IGZO Thin-Film Transistors for Low-Power Displays. *Phys. Status Solidi* **2025**, *222*, 2400894. [CrossRef]
3. Oh, I.; Park, J.; Choe, D.; Jo, J.; Jeong, H.; Jin, M.J.; Jo, Y.; Suh, J.; Min, B.C.; Yoo, J.W. A scalable molecule-based magnetic thin film for spin-thermoelectric energy conversion. *Nat. Commun.* **2021**, *12*, 1057. [CrossRef] [PubMed]
4. Alsulami, Q.A.; Rajeh, A. Modification and development in the microstructure of PVA/CMC-GO/Fe_3O_4 nanocomposites films as an application in energy storage devices and magnetic electronics industry. *Ceram. Int.* **2023**, *49*, 14399–14407. [CrossRef]

5. Geistert, K.; Pappenberger, R.; Scharfer, P.; Cavadini, P.; Schabel, W.; Sadegh, F.; Ritzer, D.B.; Abdollahi Nejand, B.; Paetzold, U.W. Spatially Regulated Gas Flow Control for Batch-Drying of Large Area Slot-Die-Coated Perovskite Thin Films. *Adv. Energy Mater.* **2025**, *15*, 2500923. [CrossRef]
6. Cho, Y.; Lee, S.; Heo, S.; Choi, S.; Bae, J.H.; Kang, I.M.; Kim, K.; Lee, W.Y.; Jang, J. Electrically and environmentally stable nitric acid-assisted SnO_2 films for the active channel layer of thin-film transistors. *Mater. Today Adv.* **2025**, *26*, 100575. [CrossRef]
7. Jaffri, S.B.; Ahmad, K.S.; Abrahams, I.; Almanqur, L.; Alharbi, Y.T.; Alderhami, S.A. N-type semiconductor [Gd_3+-Ho_3+-Dy_3+]:SnO_2 driven functionality enhancement in energy systems associated with photovoltaic and electrochemical contraptions. *Mater. Today Sustain.* **2024**, *25*, 100673. [CrossRef]
8. Kania, A.; Szindler, M.M.; Szindler, M.; Brytan, Z.; Łoński, W. Structure and Selected Properties of SnO_2 Thin Films. *Materials* **2024**, *17*, 3348. [CrossRef] [PubMed]
9. Siva Jahnavi, V.; Rajesh Babu, B.; Lakshmi, C.S. Synthesis, characterization of Al-doped SnO_2 nanoparticles for enhanced dielectric properties and antibacterial activity. *Phys. B Condens. Matter* **2024**, *692*, 416359. [CrossRef]
10. Reshma, T.; Sahu, B.K.; Panda, M.; Annalekshmi, O.; Das, A. Band edge tuned SnO_2 quantum dots allowing superoxide generation for efficient organic pollutant degradation. *J. Alloys Compd.* **2025**, *1030*, 180846. [CrossRef]
11. Chai, N.; Chen, X.; Zeng, Z.; Yu, R.; Yue, Y.; Mai, B.; Wu, J.; Mai, L.; Cheng, Y.B.; Wang, X. Photoexcitation-induced passivation of SnO_2 thin film for efficient perovskite solar cells. *Natl. Sci. Rev.* **2023**, *10*, nwad245. [CrossRef]
12. Naffouti, W.; Kamoun-Turki, N. Photocatalytic performance and solar cell simulations of TiO_2–SnO_2:F mixed oxide thin films grown by spray pyrolysis method. *Opt. Mater.* **2025**, *158*, 116491. [CrossRef]
13. Atman, B.; Karakaş, G.; Uludağ, Y. Mathematical modeling of response dynamics of n-type SnO_2-based thick film gas sensor. *Mater. Sci. Semicond. Process.* **2025**, *190*, 109360. [CrossRef]
14. Senthilkumar, P.; Raja, S.; Ramesh Babu, R.; Sriramkumar, M.; Jothivenkatachalam, K.; Vasuki, G. Enhanced optoelectronic and catalytic properties of Sm doped SnO_2 thin films. *Phys. B Condens. Matter* **2024**, *690*, 416208. [CrossRef]
15. Emam-Ismail, M.; Gharieb, A.A.; Moustafa, S.; Mahasen, M.; Shaaban, E.; El-Hagary, M. Enhancement of multifunctional optoelectronic and spintronic applications of nanostructured Cr-doped SnO_2 thin films by conducting microstructural, optical, and magnetic measurements. *J. Phys. Chem. Solids* **2021**, *157*, 110195. [CrossRef]
16. Mohajir, A.E.; Yazdi, M.A.P.; Krystianiak, A.; Heintz, O.; Martin, N.; Berger, F.; Sanchez, J.B. Nanostructuring of SnO_2 Thin Films by Associating Glancing Angle Deposition and Sputtering Pressure for Gas Sensing Applications. *Chemosensors* **2022**, *10*, 426. [CrossRef]
17. Gangwar, A.K.; Godiwal, R.; Jaiswal, J.; Baloria, V.; Pal, P.; Gupta, G.; Singh, P. Magnetron configurations dependent surface properties of SnO_2 thin films deposited by sputtering process. *Vacuum* **2020**, *177*, 109353. [CrossRef]
18. Sarica, E.; Ozcan, H.B.; Gunes, I.; Terlemezoglu, M.; Akyuz, I. Fine-tuning SnO_2 films: Unleashing their potential through deposition temperature optimization by ultrasonic spray pyrolysis. *Ceram. Int.* **2024**, *50*, 9270–9279. [CrossRef]
19. Liu, J.; Wang, Y.; Sun, Y.; Zhang, K.; Ding, Y.; Fu, C.; Wang, J. Preparation and Optimization of Mesoporous SnO_2 Quantum Dot Thin Film Gas Sensors for H_2S Detection Using XGBoost Parameter Importance Analysis. *Chemosensors* **2023**, *11*, 525. [CrossRef]
20. Kasar, R.; Deshpande, N.; Gudage, Y.; Vyas, J.; Sharma, R. Studies and correlation among the structural, optical and electrical parameters of spray-deposited tin oxide (SnO_2) thin films with different substrate temperatures. *Phys. B Condens. Matter* **2008**, *403*, 3724–3729. [CrossRef]
21. Newman, S.G. Optimizing Chemical Reactions. *Chem. Rev.* **2024**, *124*, 3645–3647. [CrossRef] [PubMed]
22. Panico, A.; Corvi, A.; Collini, L.; Sciancalepore, C. Multi objective optimization of FDM 3D printing parameters set via design of experiments and machine learning algorithms. *Sci. Rep.* **2025**, *15*, 16753. [CrossRef]
23. Antony, J. 1 - Introduction to Industrial Experimentation. In *Design of Experiments for Engineers and Scientists*, 2nd ed.; Antony, J., Ed.; Elsevier: Oxford, UK, 2014; pp. 1–6. [CrossRef]
24. Salma, S.; Hartiti, B.; Ziti, A.; Tchognia Nkuissi, H.J.; Benali, H.; Aykut, Y.; Fadili, S.; Thevenin, P.; Ertuğrul, M. Elaboration and characterization of quaternary material Cu_2ZnSnS_4 by spray pyrolysis technique using Taguchi method. *Appl. Phys. A* **2023**, *129*, 633. [CrossRef]
25. Pinheiro, X.; Vilanova, A.; Mesquita, D.; Monteiro, M.; Eriksson, J.; Barbosa, J.; Matos, C.; Oliveira, A.; Oliveira, K.; Capitão, J.; et al. Design of experiments optimization of fluorine-doped tin oxide films prepared by spray pyrolysis for photovoltaic applications. *Ceram. Int.* **2023**, *49*, 13019–13030. [CrossRef]
26. Patel, S.B.; Vaghela, G.D.; Gohel, J.V. Chapter Seven - Superior power conversion efficiency of novel solar cell and multi-response optimization of spray coated SnO_2 thin films. In *Custom Power Devices for Efficient Distributed Energy Systems*; Al-Durra, A., Raj Arya, S., K. Giri, A., Eds.; Elsevier: Amsterdam, The Netherlands, 2024; pp. 169–188. [CrossRef]
27. Zapata-Cruz, J.R.; Armendáriz-Mireles, E.N.; Rocha-Rangel, E.; Suarez-Velazquez, G.; González-Quijano, D.; Pech-Rodríguez, W.J. Implementation of Taguchi method to investigate the effect of electrophoretic deposition parameters of SnO_2 on dye sensitised solar cell performance. *Mater. Technol.* **2019**, *34*, 549–557. [CrossRef]

28. Nabizadeh Chianeh, F.; Basiri Parsa, J. Degradation of azo dye from aqueous solutions using nano-SnO_2/Ti electrode prepared by electrophoretic deposition method: Experimental Design. *Chem. Eng. Res. Des.* **2014**, *92*, 2740–2748. [CrossRef]
29. Tilebon, S.M.S.; Norouzbeigi, R. Anti-icing nano SnO_2 coated metallic surface wettability: Optimization via statistical design. *Surfaces Interfaces* **2020**, *21*, 100720. [CrossRef]
30. Fisenko, N.A.; Solomatov, I.A.; Simonenko, N.P.; Mokrushin, A.S.; Gorobtsov, P.Y.; Simonenko, T.L.; Volkov, I.A.; Simonenko, E.P.; Kuznetsov, N.T. Atmospheric Pressure Solvothermal Synthesis of Nanoscale SnO_2 and Its Application in Microextrusion Printing of a Thick-Film Chemosensor Material for Effective Ethanol Detection. *Sensors* **2022**, *22*, 9800. [CrossRef]
31. Ghamari, F.; Raoufi, D.; Arjomandi, J. Influence of thickness on crystallographic, stereometric, optoelectronic, and electrochemical characteristics of electron-beam deposited indium tin oxide thin films. *Mater. Chem. Phys.* **2021**, *260*, 124051. [CrossRef]
32. Jaishree, N.; Hashmi, A.; Katre, Y.; Singh, R.S.; Singh, J.; Srivastava, A.; Singh, A.K. The influence of different complexing agents on the properties of tin dioxide (SnO_2) deposited thin films through chemical bath approach. *Phys. B Condens. Matter* **2023**, *650*, 414520. [CrossRef]